

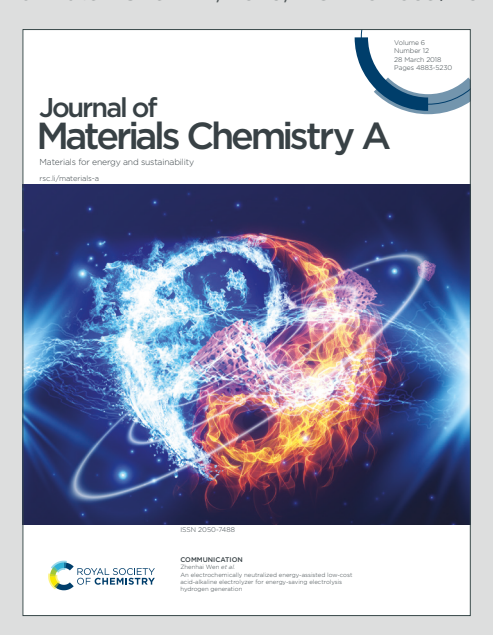
View Article Online
View Journal

Journal of Materials Chemistry A

Materials for energy and sustainability

Accepted Manuscript

This article can be cited before page numbers have been issued, to do this please use: H. Park and C. Yu, *J. Mater. Chem. A*, 2025, DOI: 10.1039/D5TA07497E.



This is an Accepted Manuscript, which has been through the Royal Society of Chemistry peer review process and has been accepted for publication.

Accepted Manuscripts are published online shortly after acceptance, before technical editing, formatting and proof reading. Using this free service, authors can make their results available to the community, in citable form, before we publish the edited article. We will replace this Accepted Manuscript with the edited and formatted Advance Article as soon as it is available.

You can find more information about Accepted Manuscripts in the <u>Information for Authors</u>.

Please note that technical editing may introduce minor changes to the text and/or graphics, which may alter content. The journal's standard <u>Terms & Conditions</u> and the <u>Ethical guidelines</u> still apply. In no event shall the Royal Society of Chemistry be held responsible for any errors or omissions in this Accepted Manuscript or any consequences arising from the use of any information it contains.



1 Simple Additive Strategy to Boost Initial Coulombic Efficiency by Mitigating

- 2 PTFE Decomposition in Dry Battery Electrodes
- 3 Hyunji Park¹ and Choongho Yu^{1,2*}
- 5 ¹ Department of Mechanical Engineering
- 6 ² Department of Materials Science and Engineering
- 7 Texas A&M University, College Station, Texas 77843 USA
- 9 *Corresponding author: chyu@tamu.edu
- 11

10

8

- 12
- 13
- 14
- 15
- 16
- 17
- 18
- 19

Abstract

Dry-processed electrodes eliminate energy/capital-intensive solvent drying processes, but indispensable polytetrafluoroethylene (PTFE) binders suffer from electrochemical reduction by lithium due to inherently low energy level of their lowest unoccupied molecular orbital (LUMO). We present a strategy to overcome this problem by elevating the LUMO with amine-containing additives, which remove the reduction signature – shoulder in voltage profiles – observed during anode lithiation. The modification, achieved via interaction between PTFE's fluorine atoms and the additive's amine group, has been validated by multiple experimental techniques and density functional theory calculations. The additive boosted both initial Coulombic efficiency and mechanical durability. Our readily implementable approach involving simple mixing of PTFE with additives opens the door for broader adoption of dry-processed electrodes, addressing one of the most significant impediments in industrialization.

34

35

36

37

38

39

40

41

42

43

44

45

46

47

48

49

50

51

52

53

54

55

Introduction

With the growth of emerging markets like electric vehicles, the market share of lithium-ion batteries (LIBs) has steadily expanded in recent years. Given this predictable growth, any method that can lower processing or material costs will significantly accelerate the application of LIBs. Among the manufacturing processes of LIBs, electrode production not only directly influences the battery's overall performance but is also one of the most cost-intensive stages, offering considerable potential for cost reduction. In the traditional electrode manufacturing process, polyvinylidene fluoride (PVDF) is commonly used as a binder, dissolved in solvents like N-Methyl-2-pyrrolidone (NMP). However, due to the high cost of NMP and its toxicity, solvent recovery is required in commercial applications, further increasing the overall cost of battery manufacturing. ¹ Regarding the solvent-related aspects during the drying process and recovery, a savings of approximately \$36.12/kWh (a 14.5% reduction) can be achieved based on a thin lithium nickel manganese cobalt oxide (NMC) electrode. ² Using water instead of toxic NMP offers significant advantages, and for the anode, water-based processes with carboxymethyl cellulose (CMC) and styrene-butadiene rubber (SBR) binders have been developed. However, from an energy perspective, water requires 2260 kJ/kg to evaporate, more than four times the 510 kJ/kg required by NMP, making it still difficult to consider it the optimal solvent. 1 By eliminating the drying process, throughput can be increased and energy consumption for heating can be reduced. ³ On top of that, the conventional solvent drying process causes the binder migration to the top surface of the electrode. ^{4,5} The binder gradient induces poor mechanical properties and blocks the pore of the top electrode surfaces, interfering to achieve the high-loading electrodes. For these reasons, eliminating solvents from the electrode manufacturing process remains a key objective for manufacturers and an area of significant research interest. ⁶

To date, quite a few manufacturing technologies for dry processed films have been reported including dry spraying deposition, 3D printing, melt stretching, powder compression, vapor deposition, and polymer fibrilization. ⁷ Specifically, the binder fibrillation method is the most promising method due to its feasibility for mass-production with roll-to-roll processes. ⁸ For the polymer fibrilization method, polytetrafluoroethylene (PTFE) is a widely used binder due to its good mechanical properties, corrosion resistance, and easy fibrilization. ⁹ Due to high electronegativity of F atoms of PTFE, the repulsive Van der Waals force between PTFE molecules is strong, which slips easily and forms PTFE fibrils under the shear force. ¹⁰ Electrodes using fibrilized PTFE binder not only have the advantage of a dry process, but also have better electrical properties with its low tortuosity compared to conventional slurry casting electrodes. Unlike wet-processed binder, which covers the surface of the active material, PTFE, which binds particles with its fibrils, does not block the surface and has a lower charge transfer resistance, facilitating fast charging. ¹¹

However, PTFE has an intrinsic problem of being easily reduced by reacting with lithium due to its low level of lowest unoccupied molecular orbital (LUMO). ^{12, 13} As the following phenomenon occurs, reductive defluorination of PTFE takes place, with the detached fluorine reacting with lithium to form LiF, while the remaining PTFE can either leave behind carbine-like carbon ¹⁴⁻¹⁶ or be terminated by hydrogen. ^{12, 17}

74
$$(CF_2)_n + 2nLi^+ + 2ne^- \rightarrow (C \equiv C)_n + 2nLiF$$
 (1)

If this reaction occurs stoichiometrically, 1072 mAh of lithium is consumed per gram of PTFE (See Note S1), which could lead to significant capacity drop. In particular, the anode exhibits inferior initial Coulombic efficiency (ICE) due to the reduced binder and experiences noticeable

capacity decay as a result of brittleness caused by degraded mechanical properties. ¹⁷⁻¹⁹ According to the news reports on Tesla's dry battery electrodes low ICE in the anode presents challenges for commercialization. However, developing alternative materials that fiberize easily and offer greater electrochemical stability than PTFE remains challenging.

An attempt to minimize PTFE content has been reported, but this is not a definitive solution and involve a trade-off with mechanical properties, which are closely tied to thickness variations. ^{11,20} Very recently, mitigating reduction of PTFE by coating the graphite active material with insulating polymers was proposed to mitigate the electrochemical degradation of PTFE and thereby undesirable lithium loss. ^{12, 21} However, the coating process of graphite particles still requires a wet process involving a solvent. More importantly, wet coating of insulating binders on the active material diminishes the advantages of the fibrous binders by minimizing their contact areas.

Herein, we propose a strategy to mitigate the inherent challenge of PTFE reduction by modulating its LUMO with additives to suppress its electrochemical decomposition. A key additive is tyramine (Ty), which contains an amine group capable of forming hydrogen bonds with PTFE through a solvent-free mixing process. In PTFE, the LUMO originates from antibonding combinations of the C2s and C2p_y orbitals, along with mixed F2p_x orbitals having anti-bonding character in the C-F bond. ^{22, 23} Hydrogen bonding can influence the electron density and enable the engineering of the band structure. ²⁴⁻²⁶ When the amine group interacts with PTFE, it redistributes electron density, thereby modulating the electronic band structure. This was confirmed by density functional theory (DFT) calculations as well as experimental results from ultraviolet-visible (UV-Vis) spectroscopy and ultraviolet photoelectron spectroscopy (UPS). The

dry-processed anode with the pristine PTFE binder exhibited a low ICE of 91.6%, indicating PTFE reduction in the first lithiation profile of the graphite half cell. In contrast, PTFE with tyramine (PTFE@Ty) suppressed the electrochemical degradation of PTFE, increasing the ICE to 94.4%. The full cell with the additive also demonstrated improved ICE and capacity retention, achieving higher specific capacities than the PTFE electrode without the additive. The electrochemical decomposition of PTFE in the absence of the additive led to fiber breakage and increased the electrode thickness, adversely affecting the cycle performance. To the best of our knowledge, this work represents the first attempt to tune the LUMO of PTFE to avoid its electrochemical degradation. This approach paves the way for mitigating the reduction of fibrous PTFE binders and enabling high energy-density, cost-effective lithium-ion batteries.

This article is licensed under a Creative Commons Attribution-NonCommercial 3.0 Unported Licence.

Open Access Article. Published on 18 November 2025. Downloaded on 11/22/2025 12:53:42 PM

111 R112 R

Results and discussions

Role of additives in modifying the electronic bands of PTFE

The inherently low LUMO level of PTFE, which lies below the Fermi level of Li metal, is the primary cause of its electrochemical decomposition. Therefore, raising the LUMO level can help mitigate this issue. Band structures can be altered through approaches like chemical doping, interatomic interactions, and mechanical strain. ²⁷⁻³⁰ Specifically, by incorporating new bonds such as covalent bonds and hydrogen bonds, the electronic structure can be adjusted. Introducing electron-donating functional groups like methoxy or amino groups enhances electron density, thereby elevating the LUMO level. ^{31,32} Utilizing an additive to form a hydrogen-bonded complex allows for modulating the electronic structure without necessitating new synthesis methods. ^{24,25}. ^{33,34} The redistribution of orbitals depends on the neighboring atoms and the extent of polarization in the hydrogen bond, which influences whether the LUMO and HOMO of the complex are lowered or raised in energy. ^{34,35} Enhancing the donor/acceptor characteristics facilitates charge transfer interactions, allowing for the reorganization of orbitals. ^{24,25,33,34}

Specifically, the C-F groups establish relatively robust intermolecular hydrogen bonds with amine groups. ³⁶ Tyramine (1-hydroxy-4-ethylaminobenzene, Ty) is a naturally occurring organic nitrogenous compound found in food, valued for its simple synthesis, low cost, and broad range of applications. The amine group of tyramine can form hydrogen bond with the fluorine atoms in PTFE. ³⁷ The C-F groups in PTFE, protected by amine groups, may also alleviate direct contact with conducting materials, thereby minimizing the electrochemical decomposition of PTFE (Figure 1(a)). As shown in Figure 1(b), DFT calculation showed that the bonding energy of PTFE and Ty is 0.155 eV and their distance is 3.427 Å, which are within the range of hydrogen bond. ^{38, 39} According to the DFT calculation results, the LUMO level of PTFE interacted with

135

136

137

138

139

140

141

142

143

144

145

146

147

148

149

150

151

152

153

154

155

tyramine is increased by 0.249 eV due to interaction (Figure S2, S3 and Table S1). The HOMO of PTFE-Ty complex originates from Ty while the LUMO is primarily from PTFE. Similarly, we explored whether small molecules with amine groups, such as melamine and benzimidazole, could form interactions similar to those of Ty. Both melamine and benzimidazole exhibit a bonding energy of 0.1 eV and an intermolecular distance of 2.5–3 Å.

Taking into account the binding energy and LUMO level, we selected Ty for further experiments to determine the LUMO of PTFE/Ty complex (PTFE@Ty). First, UPS was carried out to examine the HOMO level, while the band gap was measured using UV-Vis spectroscopy (Figure 1(c-e), S4 and S5). The HOMO (E_{HOMO}) levels were calculated using the equation, $|E_{HOMO}| = |hv - (E_{cutoff} - E_{onset})|$, where E_{cutoff} represents the intersection of the sloping line and the baseline, E_{onset} corresponds to the binding energy at the onset of the spectra, and hv denotes the energy of the incident photon from the He I source (21.2 eV). 40,41 Based on the UPS measurements, the E_{HOMO} values for PTFE and PTFE@Ty were determined to be 10.4 eV and 6.64 eV, respectively. The HOMO level of PTFE is consistent with those in the literature. ^{22, 42} To locate the LUMO level of PTFE@Ty, the band gap was found by UV-Vis spectroscopy using the Tauc plot with the equation, $(\alpha h v)^n = A(h v - E_g)$, where α is the absorption coefficient, n is 2 for indirect allowed transitions, A is a constant, and E_g represents the band gap. Given PTFE's large band gap, we adopted the previously reported band gap of 7.66 eV obtained using vacuum UV. ^{22, 43} As depicted in Figure 1(f), the experimental results indicate that Ty raises the LUMO level of PTFE beyond the work function of lithium (2.49 eV ^{44, 45}), suggesting that PTFE in combination with Ty can effectively mitigate PTFE reduction.

To assess its stability, solubility tests followed by UV-Vis spectroscopy were carried out

to see whether tyramine dissolves in a carbonate-based electrolyte, which is commonly employed in LIBs. The electrode consisting of PTFE@Ty complex and graphite did not exhibit noticeable peaks corresponding to tyramine in dimethyl carbonate solvent, whereas Ty itself primarily precipitated due to its low solubility (Figure S6). Furthermore, identical linear sweep voltammetry measurements performed both with and without tyramine within the operating voltage range of LIBs validated its electrochemical stability, showing no significant redox reactions (Figure S7). The thermal stability of the PTFE@Ty system is supported by the melting point of Tyramine (163 °C) and UPS measurements performed after hot calendaring at 80 °C, which confirm that the functional properties of the composite are preserved. Given that typical electrode processing (~40–80 °C) and operating temperatures are below this temperature, the PTFE@Ty system can be considered thermally stable under practical conditions.

168

169

170171

172

173

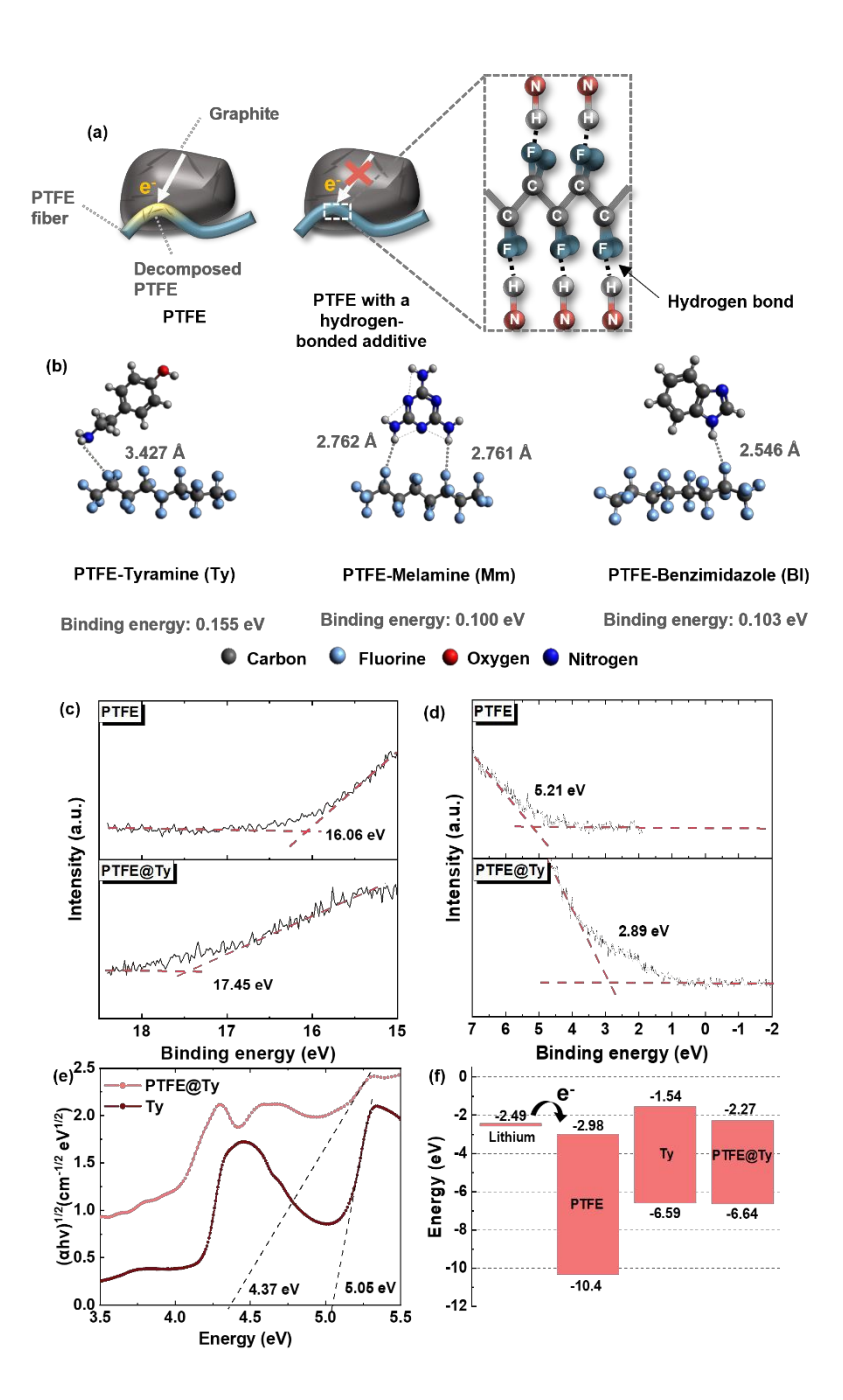


Figure 1. Modification of LUMO and HOMO levels in PTFE upon coupling with tyramine to form the PTFE-tyramine complex (PTFE@Ty). (a) Illustration of a fibrous PTFE binder in a dry-processed anode with or without the Ty additive. (b) Optimized configurations and binding energies of PTFE-Tyramine, PTFE-Melamine, and PTFE-Benzimidazole. (c) Cutoff region and (d) onset region of the UPS spectra for PTFE and PTFE@Ty (2:1 wt%). (e) Tauc plots showing the band gap derived from the UV-Vis spectra. (f) Energy level diagram of PTFE, Tyramine, and PTFE@Ty, constructed based on the UPS and UV-Vis results.

176

177

178

179

180

181

182

183

184

185

186

187

188

189

190

191

192

193

194

195

196

Interactions between PTFE and Tv

The PTFE used consists of elliptical-shaped particles with fibrous structures in between, while tyramine particles ranged from tens to hundreds of nanometers up to several microns, with larger particles exhibiting a layered structure, as observed in scanning electron microscopy (SEM) images (Figure S8 and S9). Dry mixing PTFE and tyramine under shear force increased fiber formation, with some fibers clustering into a film-like structure (Figure S10). As shown in Figure 2(a), energy-dispersive X-ray spectroscopy (EDS) mapping results reveal that nitrogen in tyramine is evenly distributed rather than clustered with slightly higher densities in the regions where F in PTFE is present. This may suggest that the mixing process disrupted intermolecular pi-pi interactions between benzene rings in tyramine, breaking it down to small fragments and likely facilitating hydrogen bond formation throughout the PTFE. The extent of PTFE reduction depends on the degree of fibrillation, as the exposed PTFE surface directly affects the reduction reaction. It is therefore important to evaluate whether Tyramine may interfere with the fibrillation process. As displayed in the SEM image of a dry-processed anode composed of PTFE@Ty and graphite, PTFE@Ty exhibits fibrous morphologies similar to those of pristine PTFE, forming long fibers with diameters ranging from tens to hundreds of nanometers, highlighting its effective role as a binder (Figure 2(b) and S11). If fibrillation were insufficient, poor electronic pathways and increased interfacial resistance would have led to a higher charge-transfer resistance. 46,47 However, the PTFE@Ty electrode with the optimized amount exhibited a comparable resistance (Figure S12), implying that the fibrillation network was well preserved.

The interactions between dry-mixed PTFE and Ty were observed by Fourier transform infrared spectroscopy (FT-IR) spectroscopy and X-ray photoelectron spectroscopy (XPS). The

198

199

200

201

202

203

204

205

206

207

208

209

210

211

212

213

214

215

216

217

PTFE peaks corresponding to the symmetric and asymmetric stretching vibrations of C-F₂ at 1142.7 and 1201.5 cm⁻¹ were blue-shifted to 1148.2 and 1202.6 cm⁻¹, respectively for the blending weight ratios of PTFE to tyramine of 5:1 (Figure 2(c)). The magnitude of the peak shift was less pronounced for the lower Ty content in PTFE@Ty (10:1) compared to PTFE@Ty (5:1). This would suggest that a higher tyramine content enables greater coverage of C-F sites in PTFE. The wagging vibration peaks at 637.4 cm⁻¹ and 623.9 cm⁻¹ also exhibited blue shifts. ^{48,49} These results could be attributed to a reduction in C-F bond lengths of PTFE due to the interactions between Ty and PTFE, as confirmed by DFT results (Figure S11). The peak at 553.6 cm⁻¹, corresponding to bending vibration, overlaps with the peak of Ty, making it difficult to discern the peak shift (Figure S14). Consistent with FT-IR results in Figure 2(c), XPS peaks corresponding to C-F₂ in both C1s and F1s spectra were also observed to shift toward higher energy. When calibrated with C-C at 284.5 eV, the peak corresponding to C-F₂ in the C1s spectra shifted from 291.1 eV to 291.9 eV with tyramine (PTFE@Ty (5:1)). Similarly, in the F1s spectrum, a peak shift from 688.4 eV to 689.1 eV was observed. These shifts toward higher energy in the XPS spectra suggest changes in the electronic environment of the PTFE due to interactions with tyramine, indicating a reduction in electron density around the C-F bonds. This is consistent with the hypothesis that tyramine interacts with and modifies the surface of PTFE, resulting in stronger binding of C-F sites by tyramine. Collectively, the FT-IR and XPS data provide robust confirmation of the chemical modifications occurring at the PTFE surface, underscoring the role of tyramine in altering the material's properties.

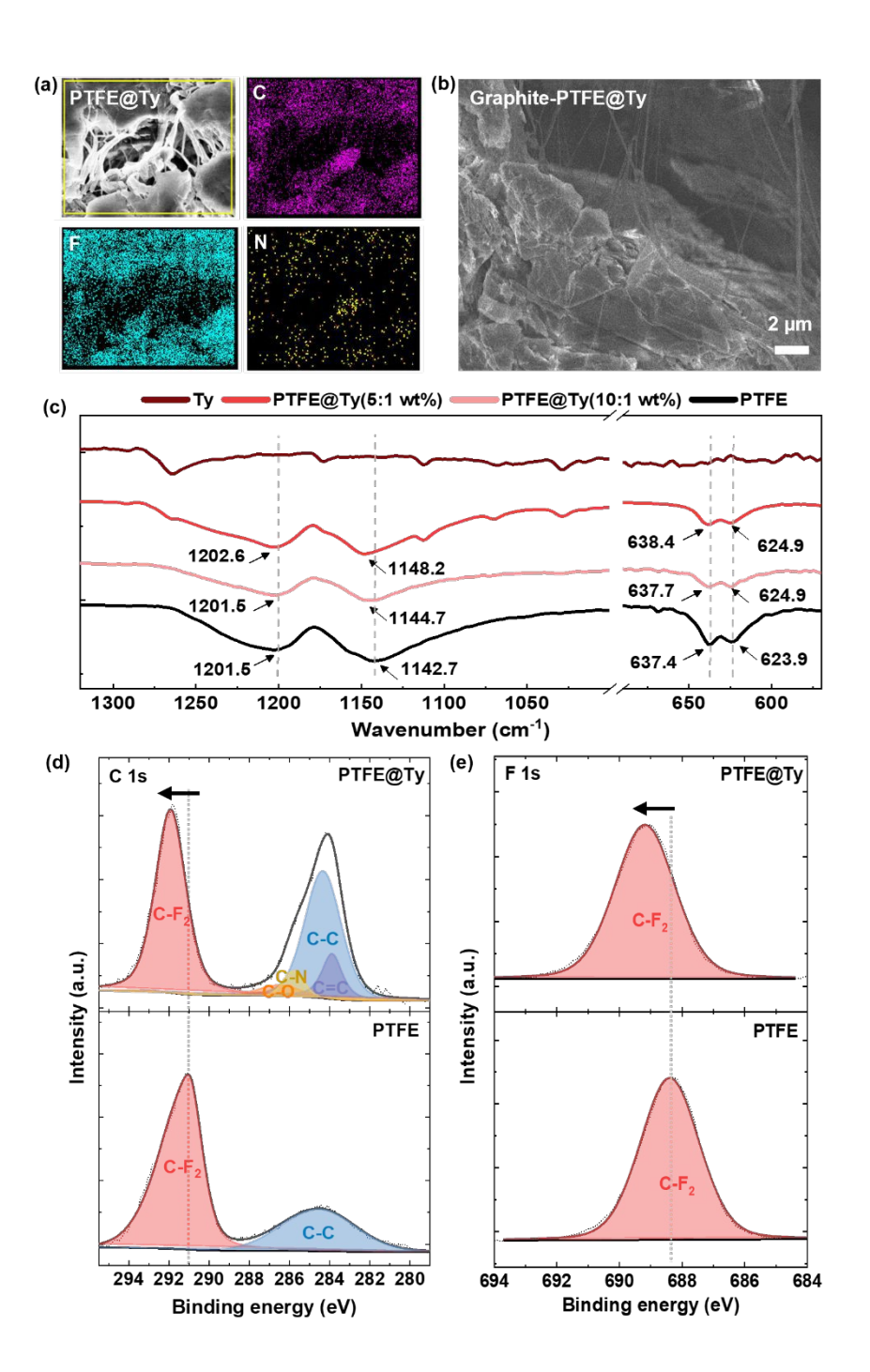


Figure 2. Experimental results on interactions between PTFE and tyramine. (a) SEM and EDS images of PTFE@Ty (5:1). (b) SEM image of an anode consisting of graphite (95 wt%) and PTFE@Ty (5:1) binder (5 wt%). (c) FT-IR spectra showing symmetric and asymmetric stretching vibrations of C-F₂ and wagging vibrations of C-F₂. XPS results of PTFE or PTFE@Ty (5:1) corresponding to (d) C 1s and (e) F 1s.

219

220221

226

227

228

229

230

231

232

233

234

235

236

237

238

239

240

241

242

243

244

245

246

Electrochemical performances

The reduction of PTFE by lithium is evidenced by changes in the voltage profile and a decrease in ICE. In the half-cell tests (Figure 3(a, b) and S15), the shoulder feature in the voltage profile, attributed to the electrochemical decomposition of 5 wt% PTFE, is distinctly observed at ~0.7 V. This decomposition results in a lower delithiation capacity and a reduced ICE of 87%. When the PTFE content was reduced to 2 wt%, the voltage shoulder became less prominent due to the reduced amount of material available for the side reactions. However, compared to the wetprocessed electrode lacking PTFE, a slight shoulder remained. In contrast, the incorporation of 0.4 wt% tyramine (PTFE@Ty) mitigated this undesirable effect, yielding a voltage profile comparable to that of a conventional anode fabricated using the wet slurry method with CMC/SBR binders. Notably, tyramine did not introduce any adverse effects, such as unwanted side reactions or increased resistance leading to higher overpotential. Consequently, the ICE of PTFE@Ty improved to 94.4%, compared to 91.6% in the absence of tyramine. To verify the general applicability of the proposed approach, the effect of tyramine was further investigated using various electrolytes, including commercial formulations (Figure S16). In all tested systems, the characteristic voltage shoulder associated with PTFE degradation during the initial charge/discharge process disappeared, accompanied by a consistent improvement in ICE. These results confirm that the beneficial effect of tyramine is not electrolyte-dependent. Based on the initial electrolyte screening, the electrolyte yielding the highest ICE was selected for subsequent electrochemical evaluations.

While reducing the PTFE content enhances ICE, it can lead to poor cycling performance, meaning it cannot be reduced indefinitely. At 5 wt%, both PTFE and PTFE@Ty exhibited good

261

262

263

264

265

266

267

268

269

cycling stability, whereas at 2 wt%, the half-cell cycle life declined slightly, and at 1 wt%, it became significantly inferior (Figure 3(c) and S17). This is because PTFE degradation compromises its ability to effectively function as a binder. In the full cells made of LiNi_{0.8}Mn_{0.1}Co_{0.1}O₂ (NMC 811) cathode and natural graphite anode (Figure 3(d) and S18), the capacity retention with 2 wt% PTFE was suboptimal likely due to a limited supply of lithium compared to half cells. However, we noticed that integrating carbon nanotube (CNT) enhances cycle life. After 50 cycles, the PTFE cell retained 78% of its initial capacity, which increased to 85% with CNT. With the incorporation of Ty into PTFE, the retention further improved to 95% with CNT. We believe the fibrous CNT network not only provides the structural reinforcement to PTFE fibers, alleviating the capacity drop caused by mechanical degradation, but also enhances electrical conductivity. 50-55 It appears that preventing structural degradation also curtails electrochemical side reactions that consume reversible lithium. Based on both ICE and capacity retention, further experiments were performed using both PTFE and CNT.

We also performed XPS measurements after the first cycle at the fully delithiated state (Figure 3(e, f)). In the F1s spectra, besides the C-F₂ peak corresponding to PTFE, a H-C-F/F-C=C peak was observed, indicating that the defluorination of C-F₂ could produce H-C-F or a carbyne structure such as F-C=C. ^{12, 19} Since LiF primarily originates from the solid electrolyte interface layer formed by LiPF₆ in the electrolyte, these findings could suggest electrochemical degradation of the binder. Here tyramine effectively maintained the larger areal ratio of C-F₂ peak relative to the H-C-F/F-C=C peak in PTFE, demonstrating a substantial suppression of the electrochemical decomposition of the binder. Tyramine enlarged C-F₂ peak area by 4.7 times with the absolute areal ratio of C-F₂ to H-C-F/F-C=C reaching 2.8 (normalized: 74%) for PTFE@Ty, compared to 0.6 (normalized: 38%) for PTFE. Similarly, in the C 1s spectra, the C-F₂ peak for PTFE@Ty

remained significantly larger than the H-C-F and F-C=C peaks, with an areal ratio of C-F₂ to H-C-F/F-C=C reaching 1.9 (normalized: 65%), compared to 0.6 (normalized: 38%) for PTFE. Although Tyramine and PTFE were thoroughly mixed, some unreacted PTFE regions are unavoidable, as inner PTFE exposed during additional fibrillation with graphite may not fully interact with Tyramine. Consequently, while minor H-C-F/F-C=C features remained, the overall defluorination was significantly suppressed compared to the pristine PTFE electrode. In addition, electrochemical impedance spectroscopy (EIS) analysis further supports this conclusion by demonstrating suppressed interfacial reactions for PTFE@Ty. Both the solid electrolyte interphase (SEI) resistances and charge-transfer resistances remained substantially lower than those of pristine PTFE after formation cycling (Figure S19), indicating that hydrogen-bond-assisted LUMO elevation effectively mitigates PTFE reduction. These results confirm that the enhancement in ICE was directly attributable to the Ty's ability to prevent PTFE decomposition.

284

285

286

287

288

289

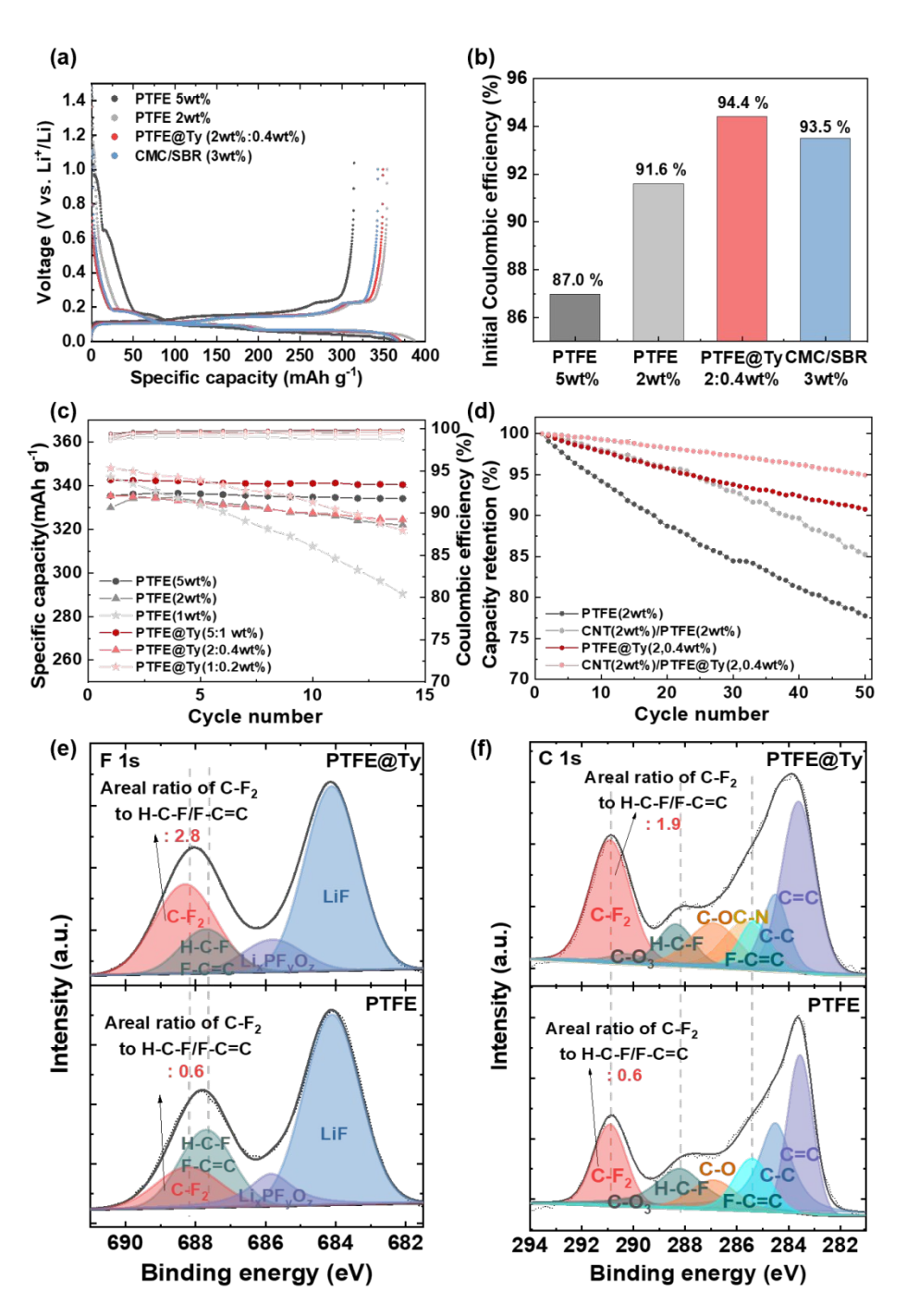


Figure 3. (a) Initial lithitation/delithiation profiles of half cells consisting of natural graphite with PTFE (5 and 2 wt%) or PTFE@Ty (2,0.4 wt%, the first number refers to the PTFE content, and the second number refers to the Tyramine content in the total electrode mass.) binder along with wet-processed electrodes containing CMC/SBR binder (3 wt%) at 0.05C. (b) Corresponding ICE of the half cells in 'a'. (c) Cycle performances (0.3C) of half cells using natural graphite depending on PTFE content and the inclusion of Ty. (d) Effects of CNT on the capacity retention of full cells (NMC811/natural graphite) at 0.3C. XPS analyses for (e) F1s and (f) C 1s spectra of the half-cell

electrodes with 2 wt% PTFE, with and without tyramine after the first cycle at 0.05C at the fully delithiated state.

We also carried out full-cell tests with wet-processed NMC 811 cathodes (Figure S20). To assess the impact of the PTFE-to-Ty ratio in a full cell configuration, we tested weight ratios of 5:1, 2:1, and 1:1 while keeping the PTFE content fixed at 2 wt% (Figure S21, 22 and 23). The 2:1 ratio resulted in a greater increase in ICE compared to the 5:1 ratio, but the further increase of tyramine (1:1 ratio) slightly reduced the ICE. The discharge capacity of the 2:1 case was considerably higher than that of the 1:1 ratio and comparable to the 5:1 ratio. While an optimal amount of tyramine effectively mitigates PTFE decomposition and enhances ICE, excessive tyramine may increase resistance, leading to capacity loss. As shown in the EIS data (Figure S11), the 2:1 ratio exhibited similar interfacial resistance compared to pristine PTFE, whereas the 1:1 ratio showed noticeably higher resistance. Therefore, the PTFE-to-Ty weight ratio of 2:1 was selected for further testing in the full cell.

The PTFE case (2 wt%) exhibited a distinct first-charge voltage profile compared to PTFE@Ty and CMC/SBR cases (Figure 4(a)), consistent with the half-cell results. It also showed a lower ICE than those of the other two cases due to lithium loss associated with PTFE reduction (Figure 4(b)). PTFE@Ty demonstrated a lifespan comparable to that of wet-processed anodes using CMC/SBR binders, confirming its effectiveness as a binder (Figure 4(c), S24, and S25). After 300 cycles at 0.5C, PTFE@Ty retained 77.7% of its capacity, whereas PTFE maintained 70.6%. EIS measurements show that both SEI and charge-transfer resistances of PTFE@Ty remain lower than those of pristine PTFE even after long-term cycling, maintaining enhanced interfacial stability and effective suppression of PTFE decomposition (Figure S26). More importantly, the inclusion of tyramine substantially suppressed electrode swelling, a critical factor in practical

315

316

317

318

319

320

321

battery operation as excessive swelling can lead to pouch or can failure and fracture. As shown in the cross-sectional image of Figure 4(d-f), the thickness of the PTFE electrode expanded from approximately 82 µm to 101 µm after 300 cycles, whereas PTFE@Ty exhibited a notably smaller increase, reaching 79 µm (Figure 4(g-i)). This suggests that PTFE, due to defluorination, was less proficient as a binder, leading to an inability to accommodate the anode's volume changes during charge-discharge cycles, which contributed to a further decline in capacity retention during the initial cycles. In contrast, PTFE@Ty maintained minimal gaps between graphite particles even after 300 cycles, with the binder fibers remaining intact and well-preserved.

323

324

325

326

327

328

329

330

331

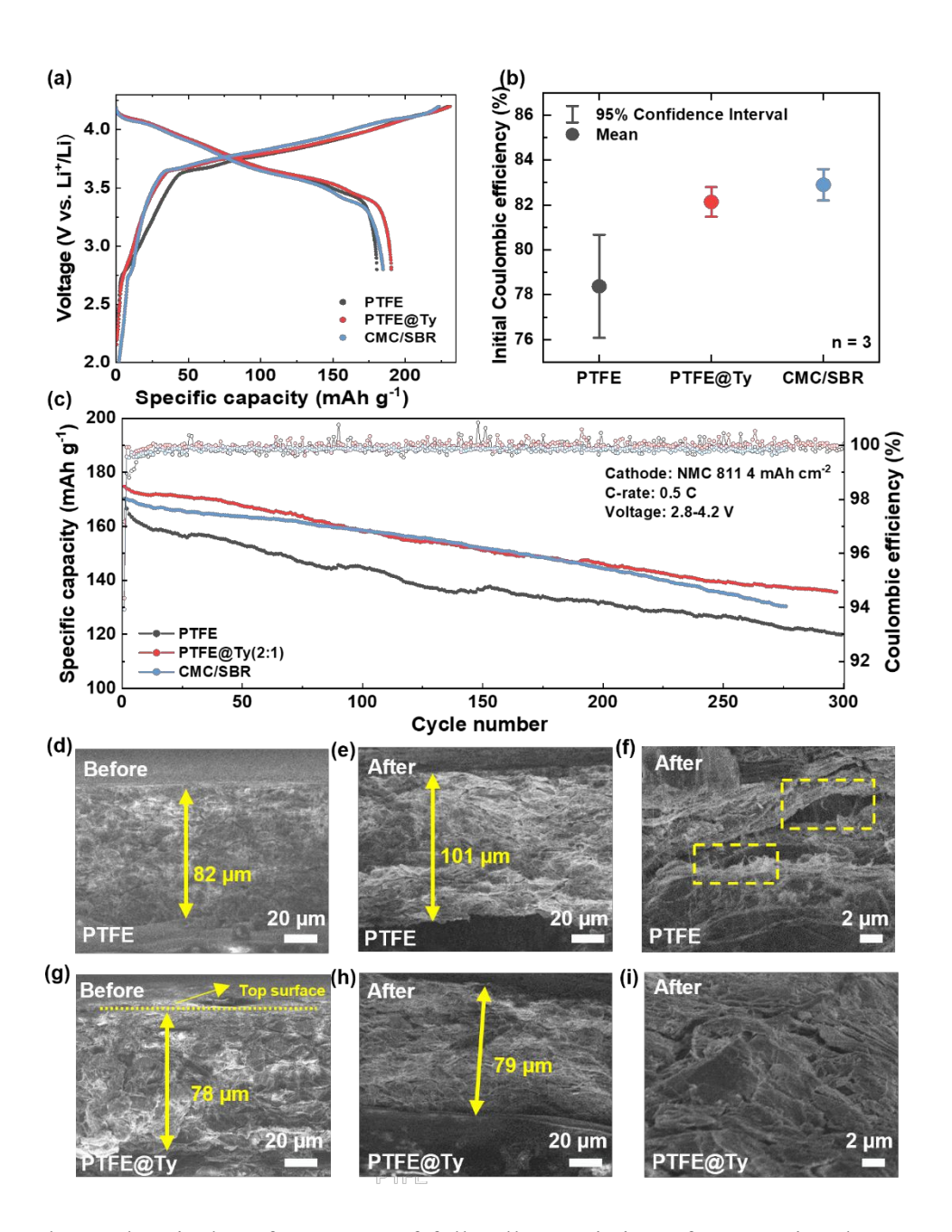


Figure 4. Electrochemical performances of full cells consisting of conventional wet-processed LiNi_{0.8}Mn_{0.1}Co_{0.1}O₂ cathodes paired with one of the three different artificial graphite anodes – dry-processed PTFE (2 wt%) and PTFE@Ty (2,1 wt%) binders, and a wet-processed CMC/SBR (3 wt%) binder. (a) Initial charge/discharge profiles at 0.05C. (b) Comparison of ICE for the full cells in 'a'. (c) Cycling performances of the full cells at 0.5C with 4 mAh cm⁻² areal capacity. Reproducibility data is provided in Figure S20. Cross-sectional SEM images of the anodes in 'c' with (d) PTFE and (g) PTFE@Ty binder before cycling; and those with (e,f) PTFE and (h,i) PTFE@Ty after 300 cycles at the fully discharged state.

Moreover, the dry-processed anode demonstrated superior rate performance compared to

333

334

335

336

337

338

339

340

341

342

343

344

345

346

347

348

349

350

351

352

353

354

Open Access Article. Published on 18 November 2025. Downloaded on 11/22/2025 12:53:42 PM.

PY-NO

This article is licensed under a Creative Commons Attribution-NonCommercial 3.0 Unported Licence.

the wet-processed anode, with the difference being more pronounced at the high current density of 2C (Figure 5(a) and S27). This difference was investigated using galvanostatic intermittent titration technique (GITT) in half cells as well as EIS in symmetric cells. In the GITT graph, PTFE@Ty exhibits an initial behavior similar to that of the wet-processed anode without the shoulder from PTFE decomposition. Figure 5(b) and S28 presented the calculated Li⁺ diffusion coefficients corresponding potential range (0.05-0.25 V) during lithium insertion into graphite, indicating improved Li⁺ diffusion on the graphite surface in the dry-processed anode compared to the wet-processed anode. Furthermore, the R_{ion} and tortuosity values obtained from EIS of the dryprocessed anodes were lower than those of conventional wet-processed anodes, enabling more effective lithium-ion transport (Figure 5(c) and Table S2). As confirmed in several studies ^{11, 56}, the fibrous PTFE binder does not obstruct the graphite surface, thus enhancing the dynamic behavior of lithium ions. With the Ty additive, these properties were further improved owing to the diminished side reactions in PTFE. The slightly higher ionic resistance observed for PTFE@Ty is likely due to the surface modification of the binder by the Tyramine additive, which marginally increases the tortuosity of ion pathways within the electrode. However, this effect is minor and does not significantly hinder overall ion transport. In contrast, the charge-transfer resistance obtained from EIS measurements after formation cycles (Figure S19) was lower for PTFE@Ty than for pristine PTFE, indicating that the suppression of PTFE reduction leads to enhanced interfacial stability and improved reaction kinetics. Consequently, the minor increase in ionic resistance is compensated by the improved charge-transfer behavior, resulting in an overall enhancement in electrochemical performance.

Elevating the LUMO level in this manner offers a readily deployable solution to the electrochemical degradation of PTFE, in contrast to earlier methods such as coating active

356

357

358

359

360

361

362

363

364

365

materials with solvents exhibiting reduced conductivity. (Table S3) Our approach achieves this objective without employing any solvents, thereby upholding the goal of eliminating solvent usage and energy/capital-intensive evaporation processes. Tyramine, a naturally derived amine commonly found in protein-rich foods and biological systems, is abundantly available and easily synthesized from inexpensive precursors, making it cost-effective and readily accessible. Its cost is comparable to that of commonly used polymer binders, indicating that it can serve as a cost-effective additive without adding significant material expense. Moreover, as it safeguards the surface of PTFE rather than the active material, it is more effectively applicable to various electrolytes and anode materials. To the best of our knowledge, this is the first endeavor to raise the LUMO of PTFE, which is expected to accelerate the commercialization of more affordable, high-energy-density dry-processed batteries.



368

369

370371

372

373

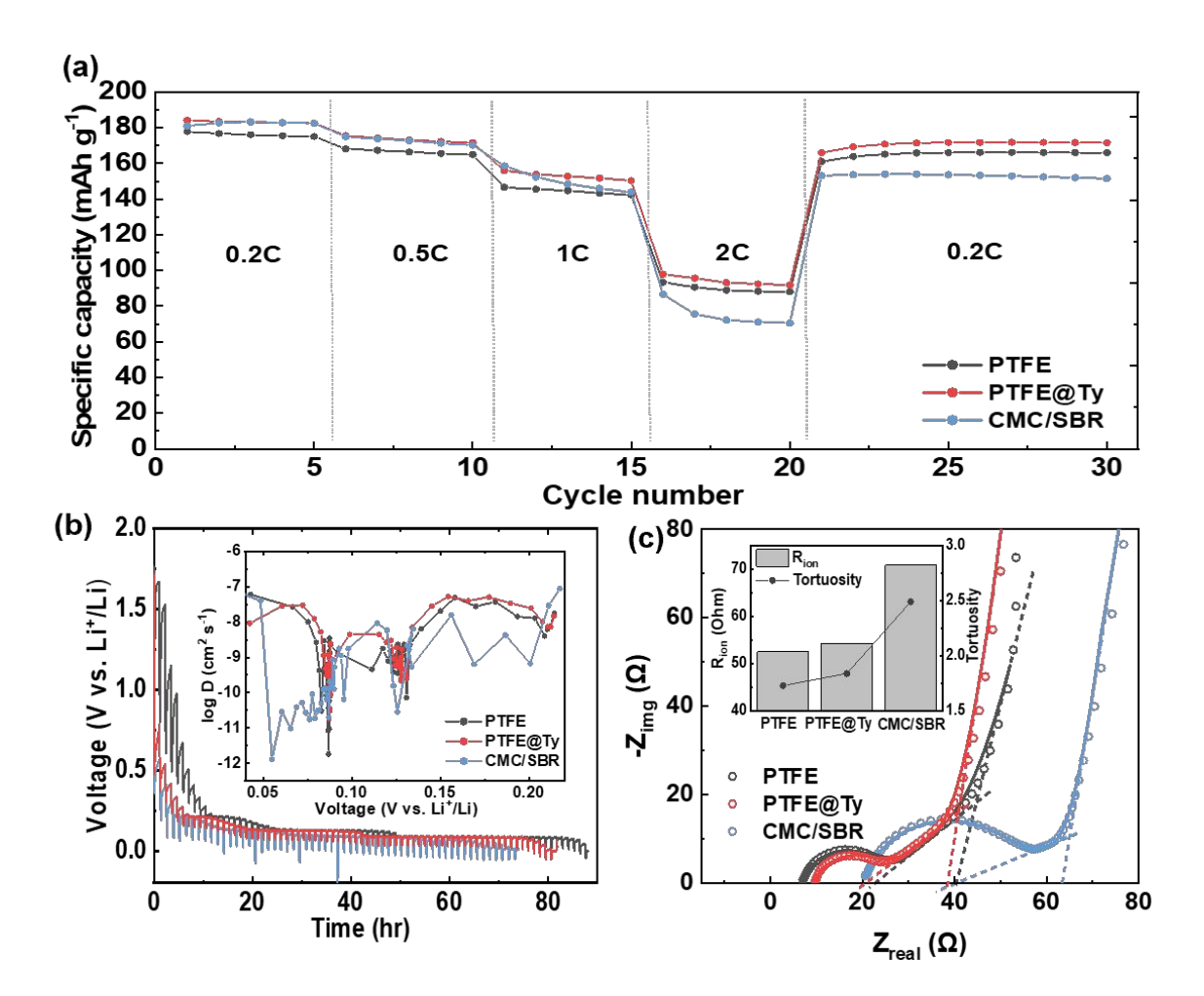


Figure 5. (a) Rate capability of full cells consisting of 4 mAh cm⁻² LiNi_{0.8}Mn_{0.1}Co_{0.1}O₂ cathodes and artificial graphite anodes using PTFE (2 wt%), PTFE@Ty (2,1 wt%), or CMC/SBR (2 wt%) binder at C-rates ranging from 0.2 to 2C (b) Galvanostatic intermittent titration-technique (GITT) test during the first lithiation process. The inset represents logarithmic values of the calculated diffusion coefficients from GITT as a function of voltage. (c) Bar graphs of R_{ion} and tortuosity obtained from the EIS data of symmetric cells with anodes prepared with PTFE (2 wt%), PTFE@Ty (2,1 wt%), or CMC/SBR (2 wt%) binder. The corresponding EIS Nyquist plots of symmetrical cells are shown in the inset.

Conclusion

We have demonstrated that the electrochemical decomposition of PTFE binder can be avoided by a readily deployable method - incorporating additive molecules bearing amine groups. The additive elevates the inherently low LUMO of PTFE, making it less prone to electron acceptance, as validated using both experimental (UPS and UV-Vis) and theoretical (DFT) results. The interaction between PTFE and Ty was supported by the DFT calculation and confirmed experimentally by FT-IR and XPS analyses. The additive boosted the ICE in half cells from 91.6% to 94.4%, as evidenced by removal of the voltage shoulder caused by the side reactions of PTFE. This mitigated unnecessary lithium loss and degradation of binder during PTFE reduction, consequently enhancing the initial discharge capacity and capacity retention in NMC811/graphite full cells. After 300 cycles at 0.5C, PTFE@Ty retained 77.7% of its initial capacity, compared to 70.6% for PTFE alone, demonstrating cycling performance comparable to that of wet process electrodes. This approach addresses a major bottleneck in the development of dry processed electrodes, paving the way for high loading, low-cost, and environmentally friendly fabrication.

396

398

399

Author contributions

- 392 Hyunji Park: conceptualization, investigation, software, data curation and writing –original draft.
- 393 Choongho Yu: conceptualization, supervision, writing review & editing.

394 Conflicts of interest

395 There are no conflicts to declare.

Data availability

The data underlying this study are available in the published article and its online ESI.

References

- D. L. Wood, J. D. Quass, J. Li, S. Ahmed, D. Ventola and C. Daniel, *Drying technology*,
 2018, 36, 234-244.
- 402 2. D. L. Wood III, J. Li and C. Daniel, *Journal of Power Sources*, 2015, **275**, 234-242.
- 403 3. Y. Lu, C.-Z. Zhao, H. Yuan, J.-K. Hu, J.-Q. Huang and Q. Zhang, *Matter*, 2022, **5**, 876-404 898.
- 405 4. M.-W. von Horstig, A. Schoo, T. Loellhoeffel, J. K. Mayer and A. Kwade, *Energy Technology*, 2022, **10**, 2200689.
- J. Klemens, L. Schneider, E. C. Herbst, N. Bohn, M. Müller, W. Bauer, P. Scharfer and W.
 Schabel, *Energy Technology*, 2022, 10, 2100985.
- 409 6. W. Jin, G. Song, J. K. Yoo, S. K. Jung, T. H. Kim and J. Kim, *ChemElectroChem*, 2024, e202400288.
- 411 7. Y. Li, Y. Wu, Z. Wang, J. Xu, T. Ma, L. Chen, H. Li and F. Wu, *Materials Today*, 2022, 55, 92-109.
- 413 8. J. Park, J. Kim, J. Kim, M. Kim, T. Song and U. Paik, *Chemical Science*, 2025, **16**, 6598-414 6619.

- 415 9. X. Wang, S. Chen, K. Zhang, L. Huang, H. Shen, Z. Chen, C. Rong, G. Wang and Z. Jiang, *Materials*, 2023, **16**, 7232.
- 417 10. K. Sato, Y. Tominaga, Y. Imai, T. Yoshiyama and Y. Aburatani, *Polymer Testing*, 2022, 418 113, 107690.
- 419 11. Y. Suh, J. K. Koo, H.-j. Im and Y.-J. Kim, *Chemical Engineering Journal*, 2023, **476**, 420 146299.
- 421 12. Z. Wei, D. Kong, L. Quan, J. He, J. Liu, Z. Tang, S. Chen, Q. Cai, R. Zhang and H. Liu, *Joule*, 2024.
- 423 13. N.-S. Choi, S.-Y. Ha, Y. Lee, J. Y. Jang, M.-H. Jeong, W. C. Shin and M. Ue, 2015.
- 424 14. L. Kavan, Chemical reviews, 1997, 97, 3061-3082.
- 425 15. G. Li, R. Xue and L. Chen, Solid State Ionics, 1996, 90, 221-225.
- 426 16. S. Shiraishi, T. Kobayashi and A. Oya, *Chemistry letters*, 2005, **34**, 1678-1679.
- J. Lee, C. Y. Son, S. Han, S. Yang, P. J. Kim, D. Lee, J. W. Lee, W.-H. Ryu and J. Choi,
 Chemical Engineering Journal, 2024, 158271.
- 429 18. Y. Zhang, F. Huld, S. Lu, C. Jektvik, F. Lou and Z. Yu, *Batteries*, 2022, **8**, 57.
- 430 19. S. Han, E.-H. Noh, S. Chae, K. Kwon, J. Lee, J.-S. Woo, S. Park, J. W. Lee, P. J. Kim and
 431 T. Song, *Journal of Energy Storage*, 2024, 96, 112693.
- 432 20. D. J. Lee, J. Jang, J. P. Lee, J. Wu, Y. T. Chen, J. Holoubek, K. Yu, S. Y. Ham, Y. Jeon
 433 and T. H. Kim, *Advanced Functional Materials*, 2023, 2301341.
- T. Lee, J. An, W. J. Chung, H. Kim, Y. Cho, H. Song, H. Lee, J. H. Kang and J. W. Choi, ACS Applied Materials & Interfaces, 2024.
- 436 22. K. Seki, H. Tanaka, T. Ohta, Y. Aoki, A. Imamura, H. Fujimoto, H. Yamamoto and H. Inokuchi, *Physica Scripta*, 1990, **41**, 167.
- T. Gumpenberger, J. Heitz, D. Bäuerle and T. Rosenmayer, *Applied Physics A*, 2005, **80**, 27-33.
- 440 24. G.-J. Zhao, B. H. Northrop, K.-L. Han and P. J. Stang, *The Journal of Physical Chemistry* 441 A, 2010, 114, 9007-9013.
- 442 25. Y. Li, F. Li and Z. Chen, *Journal of the American Chemical Society*, 2012, **134**, 11269-443 11275.
- 444 26. X. Li, L. Liu and H. B. Schlegel, *Journal of the American Chemical Society*, 2002, **124**, 9639-9647.

- D. Kang, H. Y. Lee, J.-H. Hwang, S. Jeon, D. Kim, S. Kim and S.-W. Kim, *Nano Energy*,
 2022, 100, 107531.
- 448 28. N. A. Lanzillo and C. M. Breneman, *Journal of Physics: Condensed Matter*, 2016, **28**, 325502.
- 450 29. W. Zhao, J. Ding, Y. Zou, C.-a. Di and D. Zhu, *Chemical Society Reviews*, 2020, **49**, 7210-451 7228.
- 452 30. A. Shimizu, Y. Ishizaki, S. Horiuchi, T. Hirose, K. Matsuda, H. Sato and J.-i. Yoshida, *The Journal of Organic Chemistry*, 2020, **86**, 770-781.
- 454 31. P. Morvillo and E. Bobeico, Solar Energy Materials and Solar Cells, 2008, 92, 1192-1198.
- 455 32. G. L. Eakins, J. S. Alford, B. J. Tiegs, B. E. Breyfogle and C. J. Stearman, *Journal of Physical Organic Chemistry*, 2011, **24**, 1119-1128.
- J. L. Teunissen, F. De Proft and F. De Vleeschouwer, *Journal of chemical theory and computation*, 2017, **13**, 1351-1365.
- 459 34. C. H. Liu, M. R. Niazi and D. F. Perepichka, *Angewandte Chemie International Edition*, 460 2019, **58**, 17312-17321.
- 35. C.-H. Liu, A. Wei, M. F. Cheung and D. F. Perepichka, *Chemistry of Materials*, 2022, 34, 3461-3467.
- 463 36. D. Chen, Y. Liu, C. Xia, Y. Han, Q. Sun, X. Wang, W. Chen, X. Jian, W. Lv and J. Ma,
 464 InfoMat, 2022, 4, e12247.
- Z. B. Muche, Y. Nikodimos, T. M. Tekaligne, S. K. Merso, T. Agnihotri, G. G. Serbessa,
 S.-H. Wu, W.-N. Su and B. J. Hwang, *Chemical Engineering Journal*, 2023, 476, 146400.
- 467 38. S. R. Chaudhari, S. Mogurampelly and N. Suryaprakash, *The Journal of Physical Chemistry B*, 2013, **117**, 1123-1129.
- 469 39. T. Steiner, Angewandte Chemie International Edition, 2002, 41, 48-76.
- 470 40. H. Wang, J. H. Hsu, G. Yang and C. Yu, *Advanced Materials*, 2016, **28**, 9545-9549.
- 471 41. J.-H. Hsu and C. Yu, *Nano Energy*, 2020, **67**, 104282.
- 472 42. K. Seki, R. Mitsumoto, E. Itoc, T. Araki, Y. Sakurai, D. Yoshimura, H. Ishii, Y. Ouchi, T. Miyamae and T. Narita, *Molecular Crystals and Liquid Crystals Science and Technology*.
- Section A. Molecular Crystals and Liquid Crystals, 2001, 355, 247-274.
- 475 43. K. Nagayama, T. Miyamae, R. Mitsumoto, H. Ishii, Y. Ouchi and K. Seki, *Journal of electron spectroscopy and related phenomena*, 1996, **78**, 407-410.

- 477 44. B. Alchagirov, L. K. Afaunova, F. Dyshekova and R. K. Arkhestov, *Technical Physics*, 2015, **60**, 292-299.
- 479 45. P. A. Anderson, *Physical Review*, 1949, **75**, 1205.
- 480 46. J. Hong, J. Yoon, J.-W. Park, Y.-C. Ha, J. Lee and I. Hwang, *Journal of Power Sources*, 481 2025, **655**, 237925.
- 482 47. R. Tao, B. Steinhoff, C. H. Sawicki, J. Sharma, K. Sardo, A. Bishtawi, T. Gibbs and J. Li, 483 *Journal of Power Sources*, 2023, **580**, 233379.
- 484 48. D. L. Pugmire, C. J. Wetteland, W. S. Duncan, R. E. Lakis and D. S. Schwartz, *Polymer Degradation and Stability*, 2009, **94**, 1533-1541.
- 486 49. L. Ignat'eva and V. Buznik, Russian Journal of General Chemistry, 2009, 79, 677-685.
- 487 50. H. Oh, G.-S. Kim, B. U. Hwang, J. Bang, J. Kim and K.-M. Jeong, *Chemical Engineering Journal*, 2024, **491**, 151957.
- J. Kim, K. Park, M. Kim, H. Lee, J. Choi, H. B. Park, H. Kim, J. Jang, Y. H. Kim and T.
 Song, *Advanced Energy Materials*, 2024, 14, 2303455.
- 491 52. H. Kim, J. H. Lim, T. Lee, J. An, H. Kim, H. Song, H. Lee, J. W. Choi and J. H. Kang,
 492 ACS Energy Letters, 2023, 8, 3460-3466.
- 493 53. J. K. Koo, J. Lim, J. Shin, J. K. Seo, C. Ha, W. T. A. Ran, J.-H. Lee, Y. Kwon, Y. M. Lee and Y.-J. Kim, *Energy Storage Materials*, 2025, 104270.
- J. Wang, D. Shao, Z. Fan, C. Xu, H. Dou, M. Xu, B. Ding and X. Zhang, ACS Applied
 Materials & Interfaces, 2024, 16, 26209-26216.
- 55. S. Jessl, D. Beesley, S. Engelke, C. J. Valentine, J. C. Stallard, N. Fleck, S. Ahmad, M. T. Cole and M. De Volder, *Materials Science and Engineering: A*, 2018, **735**, 269-274.
- 499 56. R. Tao, B. Steinhoff, X.-G. Sun, K. Sardo, B. Skelly, H. M. Meyer III, C. Sawicki, G. Polizos, X. Lyu and Z. Du, *Chemical Engineering Journal*, 2023, **471**, 144300.

This article is licensed under a Creative Commons Attribution-NonCommercial 3.0 Unported Licence.

Open Access Article. Published on 18 November 2025. Downloaded on 11/22/2025 12:53:42 PM.

View Article Online DOI: 10.1039/D5TA07497E

• The data supporting this article have been included as part of the Supplementary Information.